Journal of Magnetic Resonance **149,** 245–250 (2001)
doi:10.1006/jmre.2001.2301, available online at http://www.idealibrary.com on IDEAL®

Quantitation of Localized ^{31}P Magnetic Resonance Spectra Based on the Reciprocity Principle

R. Kreis,* J. Slotboom,* J. Pietz,† B. Jung,* and C. Boesch*

*Department for Clinical Research, MR Spectroscopy and Methodology, University of Berne, CH-3010 Berne, Switzerland; and †Department for Pediatric Neurology, University of Heidelberg, Heidelberg, Germany

Received November 1, 2000; revised January 30, 2001; published online March 20, 2001

There is a need for absolute quantitation methods in ^{31}P magnetic resonance spectroscopy, because none of the phosphorous-containing metabolites is necessarily constant in pathology. Here, a method for absolute quantitation of *in vivo* ^{31}P MR spectra that provides reproducible metabolite contents in institutional or standard units is described. It relies on the reciprocity principle, i.e., the proportionality between the B_1 field map and the map of reception strength for a coil with identical relative current distributions in receive and transmit mode. Cerebral tissue contents of ^{31}P metabolites were determined in a predominantly white matter-containing location in healthy subjects. The results are in good agreement with the literature and the interexamination coefficient of variance is better than that in most previous studies. A gender difference found for some of the ^{31}P metabolites may be explained by different voxel composition.

Key Words: **quantitation; brain; magnetic resonance spectroscopy; ATP; PCr; phospholipids.**

INTRODUCTION

Absolute quantitation increases the information content of clinical MR spectroscopy (MRS). For ^{1}H MRS, simple referencing to the fully relaxed water signal has turned out to be the most simple and robust way of signal calibration (*1*). As none of the phosphorous-containing metabolites can safely be assumed to be constant in pathology, there is no such convenient solution for ^{31}P MRS. This may be the main reason why in most ^{31}P MR studies to date results are reported as area ratios, with respect to either the nucleotide triphosphate (NTP) or the total phosphorous signal, which is thus assumed to be unchanged with disease. This is the case, in spite of many methods suggested for absolute quantitation, including those based on external standards (*2–4*), external reference signals (*5*), the ^{1}H water signal (*6*), the B_1-field distribution determined with ^{1}H MRI (*7*), or phantom replacement techniques with coil load matching (*8*). In the following, it is suggested that a B_1-insensitive excitation be used and that receive sensitivity be calibrated based on the reciprocity principle (*9, 10*) using a local measurement of the power required for a standardized B_1 field. Techniques relying on the reciprocity principle have been widely used in the quantitation of ^{1}H MR spectra (references in (*1*)). The suggested technique for ^{31}P MRS circumvents problems with external standards and signals, exact correspondence between ^{1}H and ^{31}P signals in double-tuned coils, and/or time consuming load matching in phantom studies for every *in vivo* measurement.

THEORY

The suggested single-voxel technique consists of two parts. As a first step, a series of ^{31}P MR spectra is recorded with a short-echo-time stimulated echo (short-TE STEAM) sequence using a range of flip angles to determine the local B_1 field. The voltage V_{max} required to obtain the maximum signal response S_{max} is taken as a measure of the local B_1 field at the region of interest (ROI), including effects of both B_1 inhomogeneities and coil loading. The ^{31}P signal can be approximated with a $\sin^3$ dependence on flip angle, i.e., B_1, or applied voltage. Strictly speaking, the $\sin^3$ dependence is only correct for a description of the stimulated echo signal strength following three hard pulses applied with sufficiently long repetition time to prevent saturation effects. For a STEAM sequence with (numerically optimized) slice-selective pulses, deviations from the nominal 90° pulse cause changes in slice profile. Similarly, pulsing too rapidly will produce saturation effects that also provoke deviations from the simple $\sin^3$ signal response. However, these effects are not detrimental, if the fitted position of the signal maximum as a function of the applied voltage is only taken as a measure of local B_1 and not taken as an indication of the 90° flip angle. Hence, the maximum signal amplitude S_{max} in this series of STEAM scans is not used in the B_1 calibration procedure, but rather the corresponding voltage V_{max} is taken as being inversely proportional to the local B_1 field. If the RF coil used is fairly homogeneous, the region selected for this calibration can be chosen larger than the real ROI in order to save time.

The final spectra to be quantitated are subsequently recorded with an ISIS sequence (*11, 12*) using adiabatic inversion and excitation pulses that yield the maximum response independent of exact knowledge of local B_1. These spectra are processed and fitted and the resonance areas can be converted to absolute units based on the reciprocity principle using the

1090-7807/01 $35.00

previously performed power calibration. The reciprocity principle *(9)*, which has recently been nicely reevaluated *(10)*, states that the signal received from a point sample in a coil following application of a pulse with a given flip angle is directly proportional to the magnetic field that is created at the position of the sample, when unit current flows through the coil. For transmit/receive coils that are matched, this relation transforms into an inverse statement between the externally applied voltage needed to achieve a certain flip angle and the receive signal induced by a local 90° pulse. The external voltage needed to produce a given B_1 field at a given location is therefore inversely proportional to the voltage induced in the coil by a predefined B_1 field occurring as a spin response. The recorded MR signals can thus be calibrated through division by the voltage $V_{\max}$ needed for the maximum STEAM signal $S_{\max}$. The units obtained by this calibration are absolute institutional units that can be used as such for direct absolute comparisons, but that need calibration measurements with solutions of known concentration to be converted to molar quantities.

The following equation contains all the factors needed for the determination of the absolute concentration c^i of metabolite i (in mmol/kg wet w),

$$c^i = \frac{A^i}{f^i_{T_1} f^i_{T_2} f_{\mathrm{CSF}} f_{\mathrm{d}} f_{B_1} f_{\mathrm{c}} f^i_{\mathrm{P}} f_T \rho}. \qquad [1]$$

A^i is the fitted peak area for metabolite i.

$f^i_{T_1}$ is the T_1 saturation correction, where the effect of the three potential ISIS inversion pulses is approximated by the effect of a single inversion pulse at the position in time of the middle inversion pulse,

$$f^i_{T_1} = \exp\{-\tau_I / T^i_1\} - \exp\{-\tau_{\mathrm{R}} / T^i_1\}, \qquad [2]$$

with τ_I being the delay between the middle inversion and the excitation pulse and τ_{R} being the relaxation delay, i.e., the time between the spoiler pulse at the end of acquisition, which was inserted for reduction of localization errors (*12*), and the following excitation pulse. Normally, $\tau_I \ll T^i_1$, such that the T_1 correction takes on the simpler, well-known exponential form.

$f^i_{T_2}$ is the T_2 saturation correction, which is minimal because of a very short dead time τ_{D} after the adiabatic half-passage excitation pulse:

$$f^i_{T_2} = \exp\{-\tau_{\mathrm{D}} / T^i_2\}. \qquad [3]$$

f_{CSF} is the correction factor to make up for the inclusion of CSF spaces. It can be determined either from MR images or a series of localized ^{1}H MR spectra with differing echo times (*13*). In the current work a constant value of 0.94 was used that had been obtained in this position from 10 healthy subjects (SD of 0.01). This correction, which is motivated by the fact that CSF does not contain relevant concentrations of most of the ^{31}P metabolites, is inadequate for inorganic phosphate (P_i), which is reported to be 0.5 mM in CSF. For P_i, the expected signal based on this assumed P_i content in CSF and the volume fraction of CSF is subtracted from the otherwise obtained concentration value.

f_{d} is the correction factor for potential changes in detector gain that is constant, if the hardware is unchanged, and can be controlled by regular phantom measurements.

f_{B_1} is the local B_1 correction factor obtained from the preceding sequence of STEAM experiments:

$$f_{B_1} = 1 / V_{\max}. \qquad [4]$$

f_{c} is a calibration constant that converts the arbitrary absolute numbers into mmol/kg using measurements on a phantom with known concentration of ^{31}P metabolites.

f^i_{P} is the number of ^{31}P nuclei in metabolite i (e.g., 3 for whole NTP pattern area or 2 for NAD).

f_T is the temperature factor to correct for unequal Boltzmann equilibrium magnetization, if calibration experiments are not performed at 38°C ($\propto 1/T$[K]).

ρ is the brain density.

Data modeling using prior knowledge constraints *(14)* is an integral part of the suggested quantification procedure. Prior knowledge enters in the form of fixed relations between different parts of the spectrum of a single component (e.g., NTP) or in the choice of model functions for broad unresolved resonances. Many model parameters were determined on summed spectra and kept at fixed relations when fitting single spectra with a much lower signal-to-noise ratio (SNR). The fitting procedure is described in more detail under Experimental.

RESULTS

The determination of the local B_1 field is illustrated for a single subject in Fig. 1. Trace a contains the average of six STEAM spectra recorded with varying flip angles and the average of the corresponding fits. The SNR of the individual spectra ranges between 20 and 50% of that of the presented sum spectrum. Figure 1b demonstrates the signal variation as a function of B_1 with the fits of all six spectra obtained with differing input power plotted on the same scale. The sum of the PCr, NTP, and P_i areas obtained from the individual spectra is plotted against B_1 in Fig. 1c, together with the modeled $\sin^3$ dependence.

Figure 2 and Table 1 portray the main results of this study. Figures 2a and 2b contain averaged ISIS spectra and the corresponding fits: in Fig. 2a for a single subject (four spectra) and in Fig. 2b for all 10 subjects (40 spectra). The fitted spectra are further illustrated in traces c and d, where the long T_2 metabolites (Fig. 2c) are separated from the broad baseline components (Fig. 2d). The adequacy of the fit model is demonstrated by the averaged residuals from all fitted spectra displayed in trace e. The concentrations obtained and their SD are

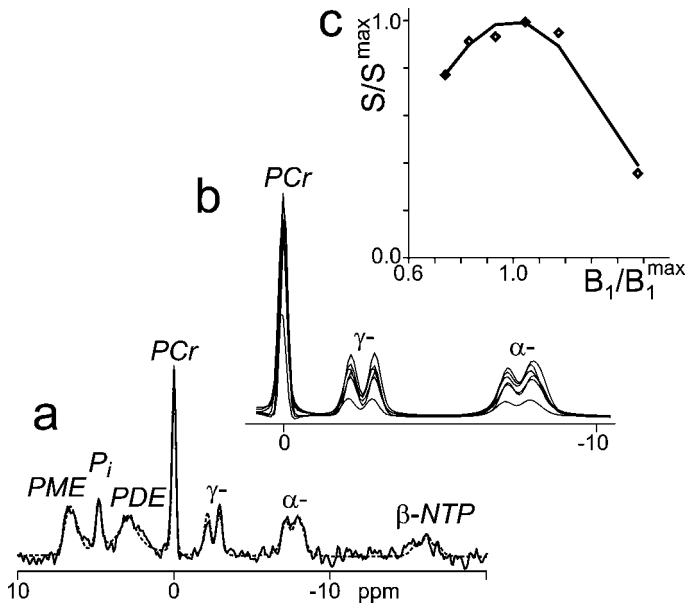

FIG. 1. Exemplary results in a single subject (female, 22 years) from the first part of the suggested quantitation method consisting of STEAM spectra recorded with varying B_1. In (a), the sum of six such spectra is plotted along with the sum of the respective fitted spectra (broken line). Trace (b) contains all six fitted spectra singly, illustrating the effect of B_1 variation on the spectra. Finally this variation is also presented in (c), where the summed signal of the PCr, NTP, and P_i areas ($\diamondsuit$) is plotted against the applied voltage, i.e., B_1, together with the modeled $\sin^3$ dependence.

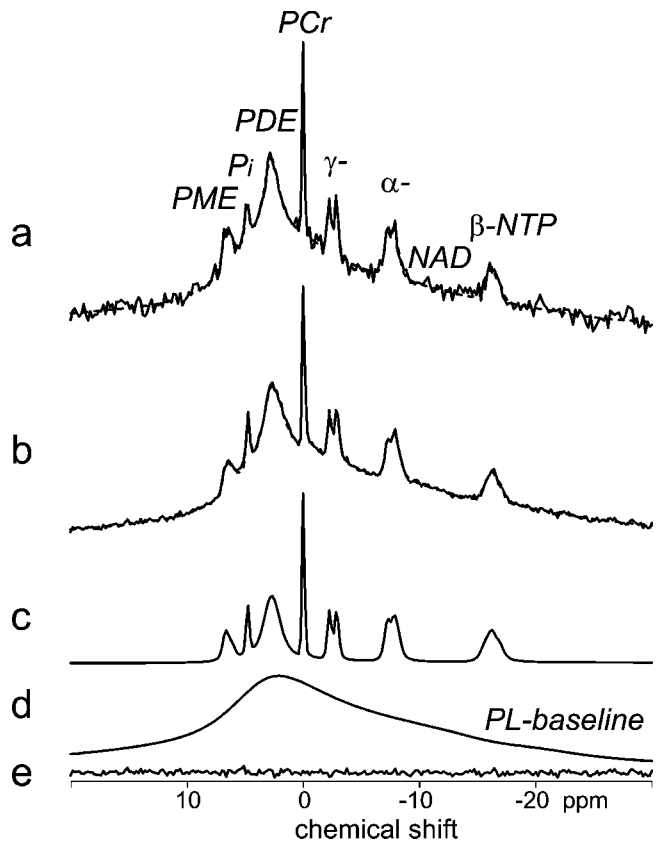

FIG. 2. ISIS-localized ^{31}P MR spectra of a cerebral ROI located predominantly in supraventricular white matter. (a) Spectrum and model fit of the same single subject as the data represented in Fig. 1. (b) Averaged spectra and model fits from 10 healthy subjects. (c) Low-molecular-weight part of the model fit containing contributions attributed to NTP, NAD, PCr, P_i, PME, and PDE. (d) Baseline components of the cerebral spectra attributed to phospholipids *(22)* and modeled as equidistantly placed Voigt lines with equal Lorentz and Gauss damping. (e) Averaged overall residuals illustrating that all reproducible spectral features are well represented by the fit model.

given in Table 1, together with the values from other studies for comparison.

Testing for gender differences (Table 2), it was found that the phosphodiester (PDE) content is on average 16% lower for women than for men ($P = 0.05$), while the ratio of phosphocreatine (PCr) vs the sum of all ^{31}P metabolites (excluding

TABLE 1

Quantitative Results of This Study Compared to Literature Values (Mean Value ± 1 SD; All Tissue Contents in mmol/kg wet wt)

Reference	PCr	NTP	P_i[a]	NAD	PME	PDE	PL-BL	Mg	pH
This study	2.72 ± 0.11	2.41 ± 0.15[b]	0.95 ± 0.09	0.20 ± 0.08	1.75 ± 0.29[c]	8.97 ± 1.29	126.1 ± 8.6	0.18 ± 0.03	7.00 ± 0.02
(8)[d]	2.8 ± 0.4	2.8 ± 0.3	1.2 ± 0.3		4.1 ± 0.8	13.6 ± 2.5			
(8)[e]	2.8 ± 0.3	2.8 ± 0.2	1.0 ± 0.2		3.1 ± 0.3	10.3 ± 1.9		0.50 ± 0.2	6.99 ± 0.02
(4)[f,g]	3.43 ± 0.14	2.97 ± 0.21			1.8	1.51			6.99 ± 0.03
(16)[h]	2.5 ± 0.3	—	0.9 ± 0.1						7.02 ± 0.02
(2)	2.9 ± 0.5	2.2 ± 0.8	1.1 ± 0.3		2.6 ± 0.8	7.7 ± 1.3			7.03 ± 0.11
(21)								0.17 ± 0.02	
(14)[g,i]				0.16 ± 0.04			22.6 ± 1.1		

[a] Contributions from CSF subtracted.
[b] 2.6 ± 0.2 mmol/kg if based on α- and β-NTP only.
[c] The relatively low value for PME found in this study is likely caused in part by the excitation profile of the adiabatic 90° pulse that had not been corrected for.
[d] White matter, i.e., similar location as this study.
[e] Cerebrum.
[f] PRESS, TE 12 ms.
[g] From proton-decoupled ^{31}P MR spectra.
[h] 84% WM, based on 2.9 mM ATP.
[i] Calculated from their published area ratio with regard to PCr and using the currently found PCr concentration.

TABLE 2

Some of the Results of This Study Grouped According to Gender (Mean Value ± 1 SEM; All Tissue Contents in mmol/kg wet wt) and *P* Values from a Univariate Repeated Measures ANOVA Including the Individual Results of the Four Repeated ISIS Spectra

	PCr	NTP	P_i	PME	PDE	Sum	PCr/sum
Female	2.74 ± 0.03	2.36 ± 0.06	0.92 ± 0.05	1.65 ± 0.14	8.20 ± 0.25	16.2 ± 0.3	0.171 ± 0.002
Male	2.70 ± 0.07	2.46 ± 0.08	0.98 ± 0.03	1.84 ± 0.11	9.73 ± 0.63	18.1 ± 0.8	0.151 ± 0.006
P value	>0.1	>0.1	>0.1	>0.1	0.05	0.06	0.01

the baseline [BL]) is significantly larger for women than for men (+13%, $P = 0.01$). All other measured tissue contents and ratios with respect to total ^{31}P metabolites were not significantly different for men and women.

DISCUSSION

The method presented allows for the determination of absolute concentrations of phosphorous-containing metabolites *in vivo*. It has the advantage that it does not necessitate the acquisition of spectra from an external standard and it also does not require calibration measurements with sophisticated phantoms or under accurately matched coil-loading conditions. Furthermore, the use of an external standard entails problems with B_1-field inhomogeneity between ROI and the position of this standard. The phantom replace technique suffers from inaccurate phantom positioning in the receive coil, while the external signal method (*5*) does not correct for inhomogeneous B_1 and may have problems with irreproducible signal pickup of the externally applied reference signal. The main price to pay in the currently suggested technique is that it requires additional *in vivo* measurements to accurately determine the local B_1 field under standardized conditions. In the current setup a series of STEAM measurements was used for this purpose. Other algorithms (*1*), which can be less time-consuming, may be used equally well. It should be noted that also in the current scheme it may be possible to use less acquisitions, pulse more rapidly, or use smaller volumes for the B_1 calibration, as it is not the amplitude ($S_{\max}$) but rather the voltage ($V_{\max}$ at $B_{1\max}$) at the maximum signal that enters the calculations. Another slight drawback of this method is that it only works with transmit/receive coils, and only those that have a reasonably constant B_1 over the localized ROI. If the applied voltage, and therefore $V_{\max}$, is measured before the final amplification stage, the nonlinearity of the high-power amplifier could influence the reciprocity correction (in the current setup an envelope feedback mechanism minimizes this effect). Furthermore, singular variations in receive sensitivity (hardware failure in the receive circuit) might be interpreted as abnormal concentrations, but this may equally well happen in other quantitation schemes.

The resulting absolute concentrations for a predominantly white matter ROI in normal subjects compare well with the values in the literature (Table 1) and the intersubject/interexamination standard deviations (SD in Table 1) are considerably lower than those in most other studies. The latter makes the technique attractive for absolute comparisons between subjects or between examinations on the same subject performed at different points in time. For this purpose, it is not even necessary to convert the initially obtained raw values in absolute institutional units to standard units which always introduces systematic errors and—if renewed calibrations are needed—also additional variation. Regular control measurements on phantoms suffice to establish constant hardware conditions over time. In the present setup it was found that over the course of half a year the hardware remained essentially constant with a coefficient of variation for the calibration measurements of 9% and without significant trends. The hardware correction factor f_d could therefore remain unchanged for the whole study.

The absolute concentrations are subject to change, if somewhat different T_1 relaxation times would have been chosen from the literature or if the effect of chemical exchange upon longitudinal relaxation (*15*) would have been included. However, it is expected that the millimolar values would not be affected by more than a 10% change for most metabolites under the experimental conditions currently used. Based on the work of Mason *et al.* (*16*), one might rather expect that a large part of the spread in published tissue contents is due to differing voxel content.

In most previous publications the phospholipid (PL) baseline (PL-BL) was not quantitated, either because it was not measured (*4*) or because it was intentionally left out of the (time-domain) fit (*8*). Indeed, one should not put much weight on the exact number also in the present study, because this certainly depends on the accuracy of the determined first-order correction, the dead time used, the obtained lineshape, and the applied T_1 and T_2 corrections (equal T_1 correction as for PDE in this study, while T_2 decay was corrected using the fitted Gauss and Lorentz decay constants). However, a coefficient of variance of 7% for this spectral component suggests that pathologic changes (as potentially involved in dys- or demyelination) might be picked up and result in clinically relevant findings. A word of caution should also be added about the concentration of PDE obtained in this and other studies using undecoupled ^{31}P MRS. Because there is a smooth transition in linewidth from the mobile PDE to the moderately mobile PL, the relative attribution of the area under these peaks to either PDE or PL is somewhat arbitrarily dependent on the assumed model.

If patients with potentially variable cerebral Mg^{2+} contents are examined, or if proton decoupling is used, the applied prior knowledge and some of the constraints would have to be modified, but this could be accommodated in the fitting program used.

In the case of ^{1}H decoupling an additional correction factor for the resulting nuclear Overhauser effect would have to be experimentally determined and included in Eq. [1] (*4*). The fitting approach used currently is particularly valuable for the evaluation of pH and Mg content, which relies on the determination of frequency differences. This is reflected by the very low standard deviations for these parameters.

In the present study, a gender difference for PDE and the ratio of PCr with respect to the summed ^{31}P metabolite content has been found. One should at this stage not draw physiologic conclusions from this finding, because the differences may either be incidental (multiple testing) or related to systematically unequal ROI content, because the ROI size was not adapted to differing head sizes. The reduced PCr and increased PDE contents for male subjects may then be related to differences in white and gray matter contributions, rather than intrinsic gender-related effects that—for the frontal lobe—have been claimed to be inverse (*17*) to what was found in the present context. A study including more subjects of either sex will be needed to clarify this issue.

In conclusion, the technique presented provides a means for obtaining quantitative ^{31}P MR spectra routinely, particularly in a clinical setting, where lengthy calibration measurements cannot be recorded for each patient. The relatively low interexamination variations should lead to a better definition of deviations with respect to the norm in individual patients and improved monitoring of changes in single subjects.

EXPERIMENTAL

All ^{31}P MR spectra were recorded on a clinical MR scanner (1.5-T Signa, General Electric) using a double-tuned bird cage ^{1}H/^{31}P head coil (quadrature for ^{31}P, linear for ^{1}H, GE Medical Systems). The ISIS sequence consisted of adiabatic full passage inversion pulses (5 ms in length) and an adiabatic half-passage excitation pulse (hyperbolic secant modulation, 2.51 ms in length) that was also reapplied after detection (*12*) . Further sequence parameters included the following: a 5000-Hz spectral width; 2048 data points; dead time $\tau_D = 80\ \mu$s; repetition time TR = 4 s *in vivo* and 2 to 30 s *in vitro*; relaxation delay $\tau_R =$ 3.58 s; and delays between the localization pulses: first to second inversion pulse 13.2 ms, second to third inversion pulse 15.2 ms, and center of third inversion pulse to end of excitation pulse 21.2 ms. PCr was placed on resonance. The excitation null of the adiabatic pulse was placed downfield of PCr outside the spectral range of interest leading to a homogeneous excitation profile for most of the spectral region of interest. However, the phosphomonoester peak might be somewhat underestimated. Cerebral spectra were recorded in 10 healthy subjects (5 male, 5 female, 26 ± 5 years) from a supraventricular ROI, placed to maximize the white matter content for a given constant nominal ROI size for the ISIS localization of 70 cm^3 (2 cm in superior/inferior direction, 5 cm in right/left direction, 7 cm in anterior/posterior direction). For the B_1 calibration with the STEAM sequence (10-ms echo time, 14-ms middle interval, 5-s repetition time) a ROI of 560 cm^3 was chosen at the same ROI coordinates (4 cm in superior/inferior direction, 10 cm in right/left direction, 14 cm in anterior/posterior direction) as for the subsequent ISIS acquisitions. The repetition time of 5 s guarantees that pathologic changes of T_1 would not translate into a misinterpretation of B_1 signal strength, as even a 50% increase in T_1 would not change the STEAM signal response by more than 5% within a range of flip angles between 45° and 135° and would leave the signal maximum at a flip angle of 90° (effect on PCr, assuming an otherwise ideal sin^3 signal response). For each subject four to six spectra of 32 scans were acquired with the STEAM sequence, usually increasing the excitation power by a factor of 1.8 around the expected signal maximum. For the ISIS scans the excitation B_1 field was chosen relative to the approximated $B_{1\,max}$, such that the adiabatic excitation produced a signal maximum for all resonances. Four spectra of 128 excitations each (total of 512 scans) were recorded. Conversion to standardized units was calibrated using a 50 mM phosphate solution (pH 7.05) at 36°C.

Data processing of the ISIS spectra included 4 Hz Gaussian broadening, Fourier transformation after data reduction to 1024 points, and constant first-order phase correction (144°), as well as automatic zero-order phasing. Spectral fitting was done with the program TDFDFIT (*18*) which performs a least-squares minimization in the frequency domain using prior knowledge constraints and a time-domain model that takes all truncation effects into account. These constraints were initially formed using an (unapodized) sum of all acquired spectra from all subjects, information from the literature *(14)*, and assumed physical constraints on linewidths, phases, and amplitudes. The model included the following resonances and constraints: PCr, the three NTP resonances (mostly from adenosine triphosphate), nicotinamide adenine dinucleotide and other dinucleotides (NAD), inorganic phosphate (P_i), phosphomonoester (PME), and PDE, as well as a model of the underlying PL baseline. All peaks were set up as one or several Voigt lines, i.e., resonances with Lorentzian (T_2) and Gaussian (lineshape) damping. A common zero-order phase was fitted for all lines. The number of lines and special constraints were as follows: PCr, Pi, single peaks with equal Gauss width; α-, β-, and γ-NTP, two doublets and one triplet with idealized symmetric intensities with equal Gauss width for its constituent lines and equal Lorentz widths for the individual phosphates; NAD, a single peak with both widths equal to the α-NTP peaks; PME, two lines with all parameters equal but separated by 14 Hz (*14*); PDE as two lines with equal position and Gauss width, but vastly different Lorentz width (sum of long T_2 and short T_2 PDE that could also be interpreted as part of the PL baseline); PL, one broad (>400 Hz Lorentz width) line centered at PCr and a sum of equally spaced lines with equal width parameters (Lorentz width >150 Hz, Gauss width >100 Hz) that were set up to model the asymmetric baseline. The least-squares sum was formed on the complex spectrum using a range of 57 ppm. Once prior knowledge was formed using the summed spectrum, the individual spectra were fitted, with the following

additional constraints: All Lorentz widths were kept constant. The coupling constants in α-, β-, and γ-NTP were fixed at the values found for the sum spectrum. The frequencies of PCr, γ-NTP, NAD, PME, and PDE were linked. Similarly the Gauss widths of PCr, all NTP lines, NAD, and PME were only allowed to vary in sync. The PL baseline components were treated as a single entity, with only one common amplitude, frequency, and Gauss width free to change.

T_1 saturation was corrected using the median of the published T_1 values listed in Ref. (*19*) (0.875, 3.14, 1.64, 1.47, and 2.5 s for NTP, PCr, PDE, P_i, and PME, respectively).

Data processing and fitting of the STEAM spectra were similar to those of the ISIS spectra. There was no first-order phase correction and the baseline was described as a single wide line. For the determination of the signal maximum as a function of input voltage, the sum of the PCr, P_i, and NTP peak areas was used. In order to get the best possible reproducibility even for low SNR the fitting model for the individual spectra included as many prior knowledge constraints as possible. For those peaks which were included in the $\sin^3$ signal fit, prior knowledge linked all frequency, phase, and width parameters (except the pH-dependent frequency of P_i).

pH was determined from the frequency difference between PCr and P_i using the equation and parameters of Petroff *et al.* (*20*). Mg^{2+} content was estimated from the frequency difference of β-NTP and PCr using the equation and parameters as published by Iotti *et al*. (*21*).

Statistical comparisons were done using unpaired two-tailed *t* tests assuming equal variance and for gender comparisons, single-factor analysis of variance with repetition.

ACKNOWLEDGMENTS

This work was supported by the Swiss National Foundation (31-43280.95) and the Medical Faculty of the University of Heidelberg (351/2000).

REFERENCES

1. R. Kreis, Quantitative localized ^{1}H-MR spectroscopy for clinical use, *Prog. NMR Spectrosc.* **31,** 155–195 (1997).
2. D. Sappey-Marinier, B. Hubesch, G. B. Matson, and M. W. Weiner, Decreased phosphorus metabolite conncentrations and alkalosis in chronic cerebral infarction, *Radiology* **182,** 29–34 (1992).
3. J. Murphy-Boesch, H. Jiang, R. Stoyanova, and T. R. Brown, Quantification of phosphorus metabolites from chemical shift imaging spectra with corrections for point spread effects and B_1 inhomogeneity, *Magn. Reson. Med.* **39,** 429–438 (1998).
4. S. Bluml, K. J. Seymour, and B. D. Ross, Developmental changes in choline- and ethanolamine-containing compounds measured with proton-decoupled ^{31}P MRS in *in vivo* human brain, *Magn. Reson. Med.* **42,** 643–654 (1999).
5. L. Barantin, A. Le Pape, and S. Akoka, A new method for absolute quantitation of MRS metabolites, *Magn. Reson. Med.* **38,** 179–182 (1997).
6. E. B. Cady, M. Wylezinska, J. Penrice, A. Lorek, and P. Amess, Quantitation of phosphorus metabolites in newborn human brain using internal water as reference standard, *Magn. Reson. Imaging* **14,** 293–304 (1996).
7. K. R. Thulborn, F. E. Boada, G. X. Shen, J. D. Christensen, and T. G. Reese, Correction of B_1 inhomogeneities using echo-planar imaging of water, *Magn. Reson. Med.* **39,** 369–375 (1998).
8. R. Buchli, C. O. Duc, E. Martin, and P. Boesiger, Assessment of absolute metabolite concentrations in human tissue by ^{31}P MRS *in vivo*. Part I. Cerebrum, cerebellum, cerebral gray and white matter, *Magn. Reson. Med.* **32,** 447–452 (1994).
9. D. I. Hoult and R. E. Richards, The signal-to-noise ratio of the nuclear magnetic resonance experiment, *J. Magn. Reson.* **24,** 71–85 (1976).
10. D. I. Hoult, The principle of reciprocity in signal strength calculations—A mathematical guide, *Concepts Magn. Reson.* **12,** 173–187 (2000).
11. R. J. Ordidge, A. Connelly, and J. A. B. Lohmann, Image-selected *in vivo* spectroscopy (ISIS). A new technique for spatially selective NMR spectroscopy, *J. Magn. Reson.* **66,** 283–294 (1986).
12. T. J. Lawry, G. S. Karczmar, M. W. Weiner, and G. B. Matson, Computer simulation of MRS localization techniques: An analysis of ISIS, *Magn. Reson. Med.* **9,** 299–314 (1989).
13. T. Ernst, R. Kreis, and B. D. Ross, Absolute quantitation of water and metabolites in the human brain. I. Compartments and water, *J. Magn. Reson. B* **102,** 1–8 (1993).
14. J. J. Potwarka, D. J. Drost, and P. C. Williamson, Quantifying ^{1}H decoupled *in vivo* ^{31}P brain spectra, *NMR Biomed*. **12,** 8–14 (1999).
15. R. G. Spencer and K. W. Fishbein, Measurement of spin–lattice relaxation times and concentrations in systems with chemical exchange using the one-pulse sequence: Breakdown of the Ernst model for partial saturation in nuclear magnetic resonance spectroscopy, *J. Magn. Reson.* **142,** 120–135 (2000).
16. G. F. Mason, W. J. Chu, J. T. Vaughan, S. L. Ponder, D. B. Twieg, D. Adams, and H. P. Hetherington, Evaluation of ^{31}P metabolite differences in human cerebral gray and white matter, *Magn. Reson. Med.* **39,** 346–353 (1998).
17. S. Riehemann, H. P. Volz, B. Wenda, G. Hubner, G. Rossger, R. Rzanny, and H. Sauer, Frontal lobe *in vivo* ^{31}P-MRS reveals gender differences in healthy controls, not in schizophrenics, *NMR Biomed*. **12,** 483–489 (1999).
18. J. Slotboom, C. Boesch, and R. Kreis, Versatile frequency domain fitting using time domain models and prior knowledge, *Magn. Reson. Med.* **39,** 899–911 (1998).
19. M. Hajek, Quantitative NMR spectroscopy.Comments on methodolgy of *in vivo* MR spectroscopy in medicine, *Q. Magn. Reson. Biol. Med.* **II,** 165–193 (1995).
20. O. A. C. Petroff, J. W. Prichard, K. L. Behar, J. R. Alger, J. A. den Hollander, and R. G. Shulman, Cerebral intracellular pH by ^{31}P nuclear magnetic resonance spectroscopy, *Neurology* **35,** 781–788 (1989).
21. S. Iotti, C. Frassineti, L. Alderighi, A. Sabatini, A. Vacca, and B. Barbiroli, *in vivo* assessment of free magnesium concentration in human brain by ^{31}P MRS. A new calibration curve based on a mathematical algorithm, *NMR Biomed*. **9,** 24–32 (1996).
22. E. J. Murphy, B. Rajagopalan, K. M. Brindle, and G. K. Radda, Phospholipid bilayer contribution to ^{31}P NMR spectra *in vivo*, *Magn. Reson. Med.* **12,** 282–289 (1989).